RGNZ/MGPB

Integrated Gravity–Seismicity Approach to Fault Mapping in the Suoh Depression, Sumatra

Rudarsko-geološko-naftni zbornik
(The Mining-Geology-Petroleum Engineering Bulletin)
DOI: 10.17794/rgn.2026.4.12

Original scientific paper

Rahmi Mulyasari[1]*, Muh Sarkowi[2], Angga Jati Widiatama[3], Hari Wiki Utama[4], Andri Kurniawan[2], Rizky J Sianturi[2]

[1] *Geological Engineering, Faculty of Engineering, Universitas Lampung, Lampung, Indonesia*
[2] *Geophysical Engineering, Faculty of Engineering, Universitas Lampung, Lampung, Indonesia*
[3] *Geological Engineering, Faculty of Industrial Technology, Institut Teknologi Sumatera, Lampung, Indonesia*
[4] *Geological Engineering, Faculty of Science and Technology, Universitas Jambi, Jambi, Indonesia*

Abstract

The Suoh Depression (West Lampung, southern Sumatra) is an active volcanic basin along the Great Sumatran Fault (GSF), characterized by high seismicity and active geothermal manifestations. This study integrates satellite gravity data and regional seismicity to delineate the subsurface fault architecture that controls deformation in Suoh. We used 3,098 gravity points from the GGMPlus model and topographic information from the 30 m SRTM DEM. Earthquake data were compiled from the BMKG catalogue (1900–2024). Gravity processing included the calculation of the complete Bouguer anomaly (CBA), separation of regional and residual components, and the application of edge-enhancement filters such as horizontal gradients and second vertical derivatives. 2-D forward modelling and 3-D density inversion were subsequently conducted to resolve the geometry of the major fault strands. Seismicity was analyzed to validate gravity-derived structures and identify active segments. The CBA varies from ~35 to ~85 mGal, reflecting major density contrasts across the Suoh basin. The West and East Semangko Faults are the two main strands of the Semangko segment, as shown by derivative maps and inversion results. Additionally, there is a local Penetoh Fault that strikes northwest and extends to a depth of about 6 km. Earthquake clusters coincide with these structures, confirming their current activity. These findings demonstrate that Suoh is an actively deforming pull-apart depression governed by strike-slip kinematics. The updated fault configuration provides critical input for seismic-hazard mitigation, geothermal assessment, and land-use planning in West Lampung.

Keywords:
Gravity methods; Great Sumatran Fault; seismicity; Suoh pull-apart basin

1. Introduction

The Great Sumatran Fault (GSF) is a big tectonic structure that runs from Aceh to Lampung. It is where the Indo-Australian and Eurasian plates meet at an angle, which causes strike-slip deformation. The GSF is a very active right-lateral fault system that causes shallow earthquakes in Sumatra. It also changes the way the region deforms, its shape, and the seismic hazards along its trace (**Irsyam et al., 2017; Hutchings & Mooney, 2021**). The Semangko segment, which is in the southern part of the system, has complicated activity because it interacts with local structures and volcanic processes in the Bukit Barisan Range.

One of the most significant deformation zones along the southern GSF is Suoh in West Lampung. This area is a pull-apart tectonic depression that formed in a releasing stepover between the Kumering and Semangko segments (**Natawidjaja, 2007**). This kind of shape causes high rates of deformation, a complicated network of fault strands, and strong geothermal activity like fumaroles, hot springs, and crater lakes (**Iqbal et al., 2023; Marwan et al., 2021**). Seismicity in this region is marked by shallow to intermediate-depth earthquakes linked to strike-slip activity and volcanic processes, establishing Suoh as a critical area for earthquake hazard evaluation.

Despite its importance, the subsurface structure of active faults in Suoh remains inconsistently mapped. This inconsistency stems from the limited visibility of outcrops and the inherent non-uniqueness of gravity data, where various geological configurations can produce analogous anomalies (**Moges et al., 2024; Hofi et al., 2024**). Thick vegetation and rough terrain make it even harder to see fault traces and rock offsets directly.

Satellite gravity models like GGMPlus work around these problems by giving you high-resolution, even coverage over difficult terrain (**Hirt et al., 2013**). To make sense of gravity data, though, you need to use strategies

* Corresponding author: Rahmi Mulyasari
e-mail address: rahmi.mulyasari@eng.unila.ac.id
Received: 30 September 2025. Accepted: 3 March 2026.
Available online: 21 July 2026

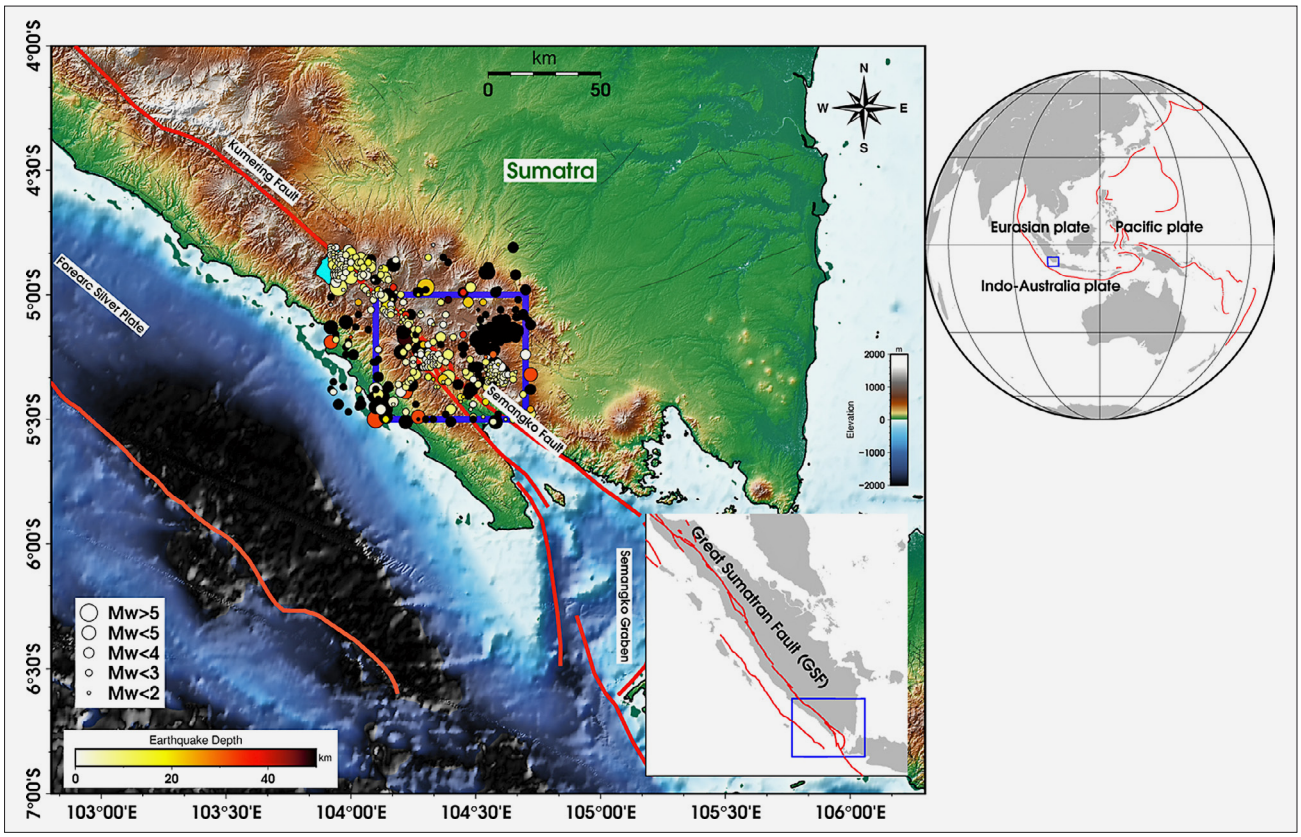


Figure 1: Seismicity and major faults in Lampung and surrounding Sumatra. The BMKG earthquake epicentres (time window given in Methods) are symbol-sized by magnitude (see legend) and colour-coded by hypocentral depth. Red lines denote the Great Sumatran Fault and the Sunda Trench; the blue dashed box outlines the Suoh study area. Basemap: SRTM15+ topography/bathymetry. The inset shows the regional plate-tectonic context. Fault traces simplified from **Sieh & Natawidjaja (2000)** and **Irsyam et al. (2017)**.

that reduce ambiguity, like gradient-based operators such as the total horizontal gradient (THG), vertical derivatives, the tilt derivative, the balanced total horizontal derivative (BTHD), and Hilbert-transform-based vertical derivatives to improve structural boundaries and show density contrasts (**Pham et al., 2024; Luo et al., 2025**). Research conducted in southern Sumatra has demonstrated that the integration of GGMPlus with contemporary edge-detection techniques, such as FSED, is effective for delineating geothermal and fault structures that are not readily discernible through surface observations (**Prasetyo et al., 2025**).

In addition to gravity, seismicity provides dynamic constraints that help identify active fault segments. By comparing gravity-derived edges with hypocenter distributions, it is possible to tell the difference between active faults and lithologic boundaries that are not active. Integrated gravity-seismic methods have been successful in Sumatra and Southeast Asia for locating blind faults, assessing segment continuity, and elucidating structural controls on geothermal manifestations (**Abdelrahman et al., 2024; Dewanto et al., 2022; Pranata et al., 2023; Supendi et al., 2023; Yanis et al., 2023**).

In light of this context, the current study concentrates on delineating active structures in Suoh by employing high-resolution GGMPlus satellite gravity, gradient analysis, 2-D gravity forward modelling, 3-D density inversion, and regional seismicity analysis. The objectives of this study are to: (1) define the boundaries and segmentation of active faults in the Suoh Depression; (2) assess the efficacy of various gradient operators in identifying tectonically significant density boundaries; and (3) generate an updated active fault map that facilitates earthquake hazard assessment and geothermal system evaluation in West Lampung. The main contribution of this study is the development of an explicit and reproducible integrated workflow that reduces the non-uniqueness of gravity interpretation in a structurally and volcanically complex environment such as Suoh.

2. Regional Geology

Suoh is on the GSF, which is a dextral fault system that runs from NW to SE. A dextral fault is one where the block on the other side moves right from the observer's view. This type of movement is the most common in Sumatra's tectonic framework. The Kumering segment to the northeast and the Semangko segment to the west-south make a stepover in this area. This interaction creates a long tectonic depression with clear structural lineaments

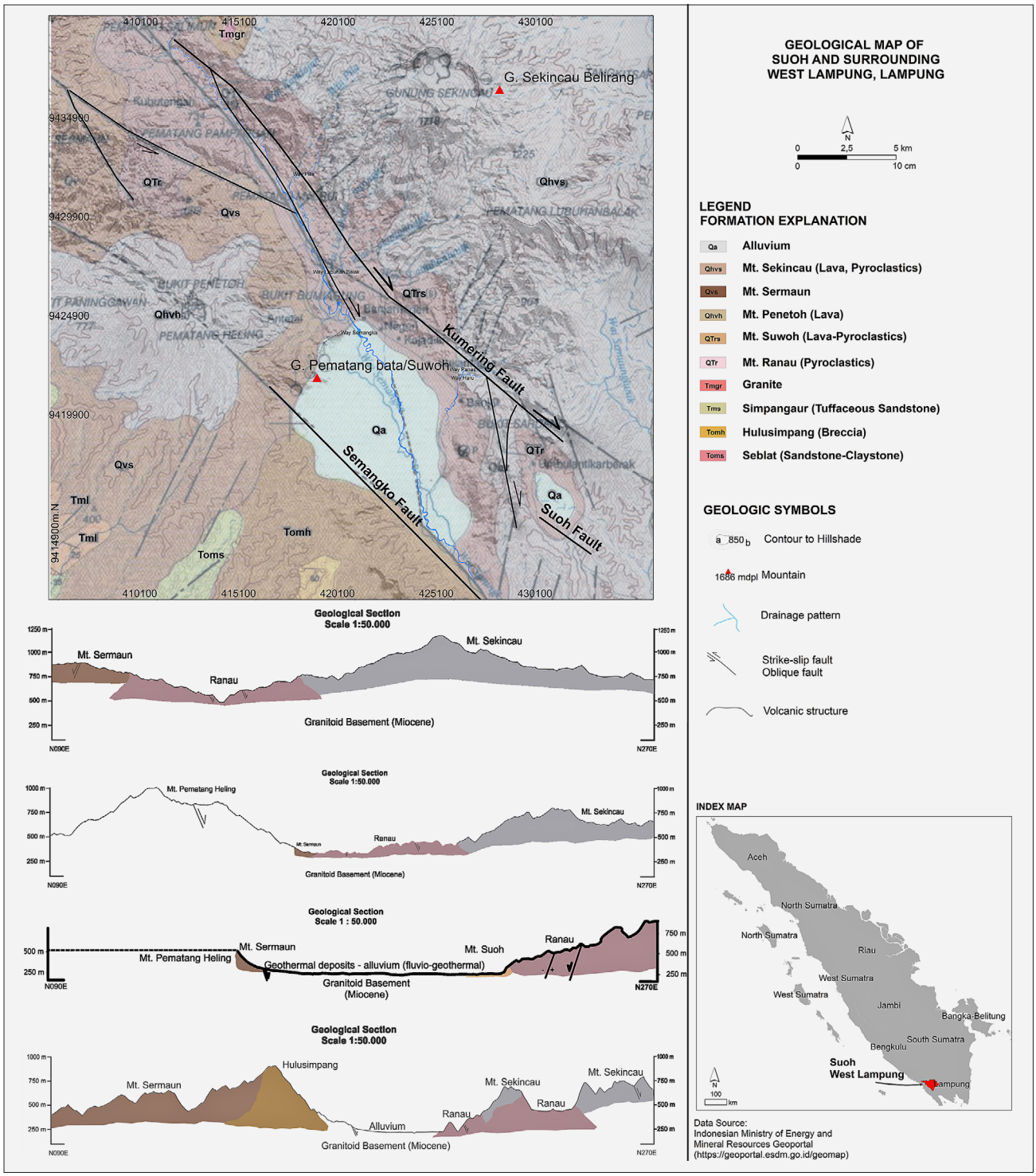


Figure 2: Geological map of the Suoh area, West Lampung (modified after **Amin et al., 1993**). Tertiary–Quaternary units include the Hulusimpang, Seblat, Simpangaur, and Ranau formations, overlain by Quaternary volcanic rocks and young alluvium. Thick lines trace the Semangko segment of the Great Sumatran Fault (West and East Semangko strands) and subsidiary faults; dashed outlines mark the Suoh grabens. The stratigraphic column and generalised section (right) summarise unit relationships and basin architectures. See the legend for symbols and scale.

(**Natawidjaja, 2007; Sarkowi et al., 2022**). The composite fault zone is linked to a lot of deformation and earthquakes, both in the past and now (see **Figure 1**).

Dextral overlap/overstep between the Kumering and Semangko segments facilitates the development of the Ranau–Suoh pull-apart. Geometric discontinuities (restraining or releasing sections) and zones where the fault trace locally bends to create areas of compression (restraining) or extension (releasing) act as barriers and triggers for rupture propagation while also focusing hy-

drothermal fluid pathways along zones of elevated permeability (**Bellier et al., 1997**). Neotectonic and paleoseismic evidence for fine-scale segmentation explains why some sub-segments are seismically active while others appear comparatively quiescent on decadal timescales (**Sieh & Natawidjaja, 2000; Burton & Hall, 2014**). Within this framework, Suoh evolved first as a subsiding basin formed by the overlap of the two GSF segments and deepened through time; a linking strand, the Suoh Fault, subsequently developed between the segments and, together with the Semangko segment, produced a younger and shallower pull-apart depression (**Putra & Husein, 2016**) (see **Figure 2**). This step-over architecture governs not only fault segmentation but also fluid migration in the Quaternary volcanic setting.

Historically, the February 15, 1994 Mw 6.8 Liwa earthquake is a key event on the Semangko segment within a complex, arc-related fault network (**Widiwijayanti et al., 1996**). Since 1994, small-to-moderate earthquakes have clustered along several Semangko sub-segments, aligned with positive structural zones (transfer zones), highlighting the role of segmentation in stress accumulation and release (**Supendi et al., 2022**). Regionally, the Ranau–Suoh corridor ranks among Indonesia's most active (**Hutchings & Mooney, 2021**) and is a focus area in the national seismic source and hazard map (**Irsyam et al., 2017**).

The West Lampung area, including Suoh, comprises Tertiary to Quaternary units: the Hulusimpang, Seblat, Simpangaur, and Ranau formations, overlain by Quaternary volcanic rocks and young alluvium (**Amin et al., 1993**). Key lithologies include andesitic lavas, volcanic and pumice breccias, tuffs, and local limestones, together with hydrothermal alteration products that commonly exhibit high permeability. This lithologic assemblage produces pronounced density contrasts and mechanical heterogeneity, which are advantageous for gravity-based mapping of structural boundaries (**Wibowo et al., 2022**).

The dominant NW–SE fault traces are intersected by near-orthogonal secondary structures, generating elongated surface fractures, steep basin margins, and clusters of geothermal manifestations (hot springs, fumaroles) along high-lineament corridors. Satellite imagery and lineament analysis indicate high fault density, particularly around Lake Suoh and Penetoh Hill, consistent with structure-controlled permeability in an active tectono-volcanic system (**Iqbal & Juliarka, 2019; Zaenudin et al., 2021**). Complete and residual Bouguer anomalies, which represent gravity values corrected for topography and separated into regional and local components, vary systematically along the NW–SE trend and match the GSF framework. Derivative-based edge indicators such as the First Horizontal Derivative (FHD), which enhances lateral density contrasts, and the Second Vertical Derivative (SVD), which sharpens shallow anomaly sources, highlight several candidate boundaries interpreted as active structures that govern the local geological architecture (**Zaenudin et al., 2021; Wibowo et al., 2022**).

3. Materials and Methods

This study aims to refine the delineation of active faults in Suoh, West Lampung, Sumatra, by integrating gravity, topographic, seismicity, and geological data. Four primary datasets were compiled for this purpose. First, satellite gravity data from the GGMPlus model (sourced from https://murray-lab.caltech.edu/GGMplus/index.html) sampled at 3,098 points with approximately 200 m spacing, were used to resolve lateral density variations associated with subsurface structures. Second, the 30 m SRTM Digital Elevation Model (DEM) provided terrain information required for Bouguer corrections and for assessing geomorphological lineaments. Third, earthquake records from the BMKG catalogue supplied regional seismicity patterns that help identify active deformation zones. Finally, lithological and structural context was obtained from the 1:250,000 Geological Map of the Kota Agung sheet (**Amin et al., 1993**). All datasets were projected to WGS84/UTM Zone 48S and resampled to a uniform 200 m grid to ensure consistency during subsequent gravity modelling and gradient-based structural analysis.

Gravity processing was conducted to produce the Complete Bouguer Anomaly (CBA), which represents gravity values corrected for elevation, topographic mass, and terrain effects. The CBA serves as the foundation for identifying density contrasts associated with faults and lithologic boundaries. Surface rock density was estimated by Parasnis regression (free-air anomaly vs. Bouguer correction) over lithologically homogeneous areas, yielding an effective Bouguer density of $\rho \approx 2.4$ g cm^{-3} (**Parasnis, 1967; Telford et al., 1990**). Normal gravity was computed using Moritz's formulation; free-air and Bouguer corrections were then applied, followed by curvature and terrain corrections (**LaFehr, 1991; Nowell, 1999; Rollin, 1990; Sarkowi, 2014**). For clarity, the key equations are summarised below.

Normal gravity (**Moritz, 2000**) (**Equation 1**):

$$g_\varphi = 978.032{,}7(1 + 5.3024\ 10^{-3}\ Sin^2\varphi - \\ - 5{,}8\ 10^{-6}\ Sin^2\ 2\phi) \quad (1)$$

Bouguer slab (Bullard A; LaFehr's constant) (**Equation 2**):

$$Bc = 2\pi G\rho h = 0.04193\rho h \quad (2)$$

where ρ is the average density (g cm^{-3}) and h is elevation (m).

CBA is defined as (**Equation 3** and **Equation 4**):

$$\Delta g(x,y,z) = g_{obs} - \left(g_{(\phi)} - FAC + BC - TC\right) \quad (3)$$

$$g(x,y,z) = g_{obs} - g_{(\phi)} + 0{,}308765h - \\ - 0.04193\rho h + TC \quad (4)$$

with FA the free-air term (0.308765 mGal m^{-1}), BC the Bouguer correction, and TC the terrain correction derived from SRTM.

To isolate near-surface anomalies, the CBA field was separated into regional and residual components using a moving-average filter with a cut-off radius chosen based on sensitivity testing (**Izvoltova et al., 2022**). Residual anomalies highlight shallow density variations associated with faulting, basin-fill distributions, or intrusive contacts.

To enhance density boundaries associated with faults and formation contacts, we computed derivative-based edge detection methods that were applied to the residual field to sharpen fault-related boundaries. These include First Horizontal Derivative (FHD): enhances lateral density changes, Second Horizontal Derivative (SHD): emphasises shallow, high-frequency sources, Second Vertical Derivative (SVD): highly sensitive to near-surface density contrasts on the residual field (**Elkins, 1951; Al-Khafaji, 2017; Saibi et al., 2006; Sarkowi, 2010; Sumintadireja et al., 2018; Sarkowi & Wibowo, 2021**). Discrete formulations are used in this study.

First horizontal derivative (component form) (**Equation 5**):

$$SFHD = FHDx + FHDy \tag{5}$$

SFHD : Sum of First Horizontal Derivatives

FHD : First Horizontal Derivative

With: $FHDx = \frac{\Delta g}{\Delta x} = \frac{g_2 - g_1}{x_2 - x_1}$ and $FHDy = \frac{\Delta g}{\Delta y} = \frac{g_2 - g_1}{y - y_1}$

Second horizontal derivative (**Equation 6**):

$$SSHD = SHDx + SHDy \tag{6}$$

SSHD = Sum of Second Horizontal Derivatives

SHD = Second Horizontal Derivatives

With: $SHDx = \frac{FHDx_2 - FHDx_1}{\Delta x}$ and $SHDy = \frac{FHDy_2 - FHDy_1}{\Delta y}$

Second vertical derivative (from Laplace's equation) (**Equation 7** and **Equation 8**):

$$\nabla^2 \Delta g = 0 \text{ or } \frac{\partial^2 \Delta g}{\partial x^2} + \frac{\partial^2 \Delta g}{\partial y^2} + \frac{\partial^2 \Delta g}{\partial z^2} = 0 \tag{7}$$

$$\frac{\partial^2 \Delta g}{\partial z^2} = -\frac{\partial^2 \Delta g}{\partial x^2} + \frac{\partial^2 \Delta g}{\partial y^2} \tag{8}$$

The maxima and minima in SFHD, zero crossings in SSHD, and instances where SVD equals zero were collectively used to delineate lateral density contrasts that are interpreted as structural edges. BMKG earthquake data within the study area were extracted, quality-checked, and restricted to crustal depths (≤ 40 km). To minimise catalogue bias, only events above the magnitude completeness threshold (Mc), defined as the smallest magnitude reliably detected, were retained, and duplicate or poorly constrained events were removed. Although double-difference relocation can improve hypocentre precision, it was not applied due to limitations of the available dataset. Seismicity was integrated with gravity-derived edges using two complementary approaches: (i) qualitative comparison of epicentre patterns with gravity edges; (ii) quantitative proximity analysis that computes the distance of each event to the nearest edge using fixed buffers (e.g. 1–2 km). Summary statistics (median and inter-percentile range) are reported to characterise clustering along structural boundaries.

Representative transects crossing major edges were modelled using two-dimensional forward gravity modelling (**Salem et al., 2014**). For volumetric imaging, three-dimensional density inversion of the residual gravity field was performed using the GRAV3D software package (UBC-GIF) to produce a subsurface density model (**Witter et al., 2016; Nyalugwe et al., 2020**). The inversion incorporated depth weighting, smoothness constraints, and density bounds consistent with the regional geology. Modelling parameters, including cell size, padding, misfit targets, error floor, and stopping criteria, are reported with the results. Depth slices and vertical sections from the inversion were compared with mapped edges and seismicity patterns to assess structural consistency.

Validation consisted of evaluating spatial agreement between gravity-derived edges and mapped geological boundaries, analysing the proximity of seismicity clusters to the identified edges, and testing the stability of edge positions under variations in filtering windows and gradient operator parameters. Uncertainty in edge location is represented by differences among gradient operators, while uncertainty in the density model is conveyed through inversion misfit statistics and consistency across structural profiles.

4. Results and Discussion

4.1. Complete Bouguer Anomaly (CBA)

The CBA map of Suoh exhibits pronounced gravity variations at a regional scale that correlate with mapped tectonic structures (see **Figure 3**). Values range from approximately 35 mGal (low; blue–violet on the colour scale) to about 85 mGal (high; red–orange), indicating strong lateral density contrasts at structural depths.

A prominent high-anomaly domain occupies the southwestern part of the area and coincides with topographic highs (Paninggawan and Penetoh hills). These highs are consistent with shallow, relatively dense bodies, such as uplifted basement, shallow intrusive rocks, or compacted volcanic units, approaching the observation level and producing local gravity increases. In contrast, a broad low-anomaly field in the northeast around Mount Sekincau suggests lower-density material or mechanically weakened/altered zones, plausibly related to hydrothermal alteration, young volcanic deposits, or fluid-bearing reservoirs.

The principal lateral gradient separating the high and low domains aligns with the Great Sumatran Fault (Semangko segment), which therefore marks the main grav-

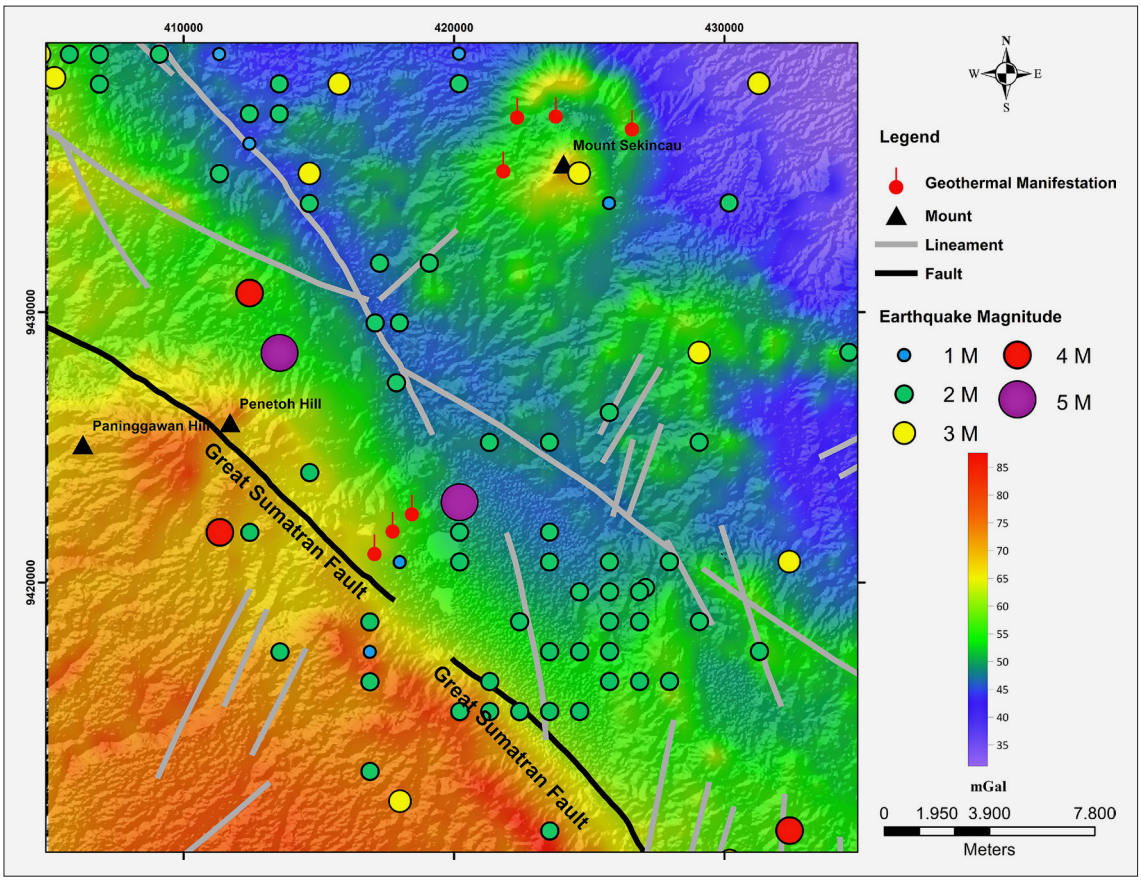


Figure 3: The Complete Bouguer Anomaly Map of the Study Area.

ity boundary: denser rocks to the west and less-dense rocks to the east. Oblique and subparallel secondary lineaments intersect this boundary, defining a complex structural fabric that likely localises strain and channels deformation and fluid flow.

Overall, the CBA pattern reinforces the view that fault architecture exerts first-order control on regional morphology and indicates an actively deforming zone. In concert with the historical seismic record for West Lampung, these contrasts highlight a significant earthquake hazard in the Suoh area.

4.2. Residual Bouguer anomalies

The residual Bouguer anomaly over Suoh ranges from roughly −4 to +22 mGal and emphasises shallow sources (see **Figure 4**). High residuals (yellow–red) cluster around Mount Sekincau, forming a rounded pattern indicative of a relatively shallow, dense body – consistent with an intrusion or compact volcanic unit.

In contrast, low residuals (blue–purple) dominate the central to southern sector, particularly along the trace of the Great Sumatran Fault (Semangko segment). These lows are interpreted as zones of reduced density produced by fracturing, tectonic weakening, and/or alteration, and they align with mapped faults and lineaments. The correspondence between low anomalies and fault trends suggests structurally controlled weak zones that are prone to strain accumulation. Taken together, the residual field supports an actively deforming setting: low-density corridors coincide with active faulting and likely mark loci for future seismic energy release, underscoring elevated earthquake hazard across the Suoh corridor.

4.3. Second Vertical Derivative (SVD)

The SVD map over Suoh highlights second-order variations that sharpen lateral density boundaries (see **Figure 5**). The dashed contours mark SVD = 0, which by definition separates positive from negative curvature and commonly coincides with significant density contrasts; in gravity interpretation, these zero lines are diagnostic of major faults or lithologic contacts.

In map view, SVD = 0 aligns with the Great Sumatran Fault (Semangko segment) and with NW–SE and NE–SW lineaments, indicating that the master fault and its splays exert primary control on subsurface architecture. Intersections among these trends outline a complex deformation network that can localise strain and act as sources of seismic energy release.

Elevated SVD amplitudes (from green to red) cluster around volcanic centres such as Mount Sekincau, Paninggawan Hill, and Penetoh Hill, consistent with compact intrusive or volcanic bodies of relatively high den-

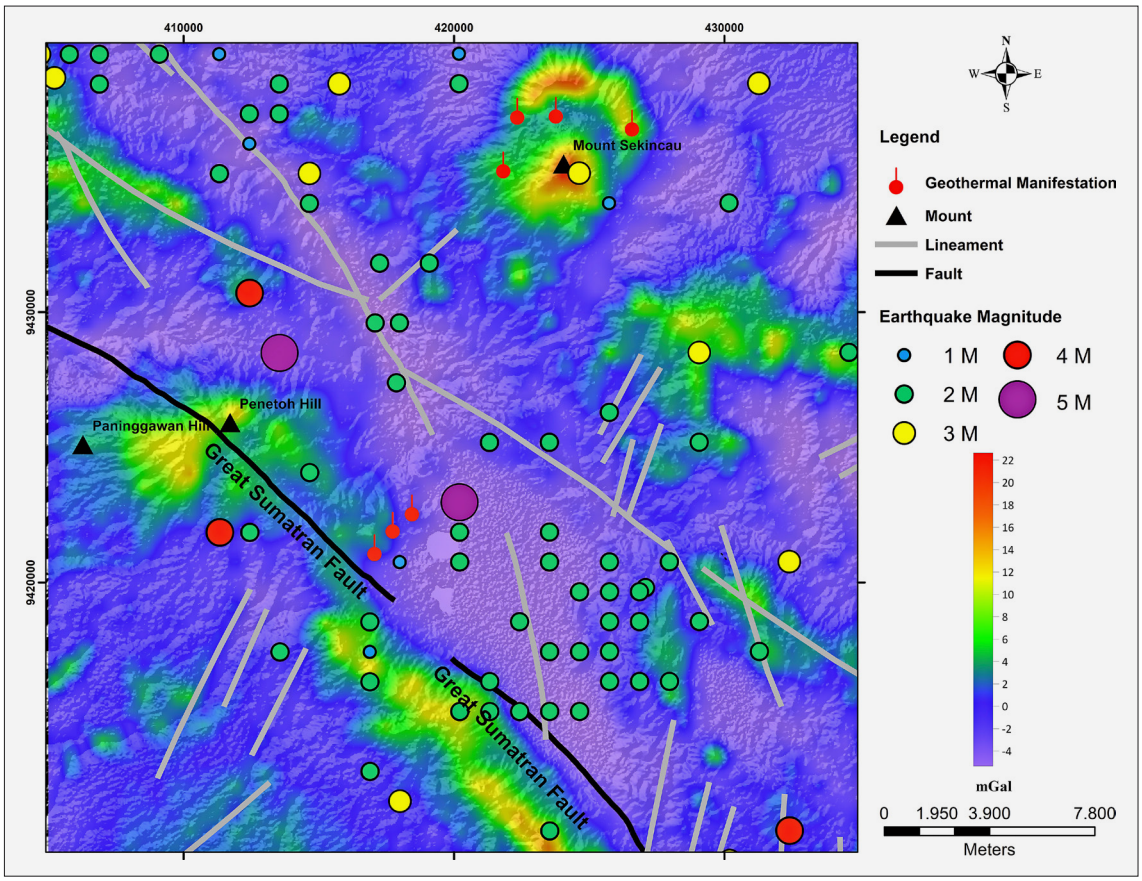


Figure 4: Residual Anomaly Map of the Study Area.

sity at shallow depths. Conversely, low SVD values (blue–purple) dominate depression zones adjacent to the fault strands and likely reflect unconsolidated sediments or mechanically weakened rocks. Together, the concentration of high SVD near volcanic edifices and the SVD = 0 traces along the main fault confirm intense tectonic activity and a strong structural control on the present-day deformation field in Suoh.

4.4. Suoh depression map

The depression map delineates a set of fault-bounded basins (see black dashed outlines in **Figure 6**). These elongate depressions parallel the Semangko segment of the GSF and its subsidiary lineaments, consistent with formation by extension and strike-slip step-over, ranging from small grabens to pull-apart basins. The Suoh basin was formed as a result of an overstep mechanism between two active fault segments, namely the Semangko segment and the Kumering segment. When these two segments moved dextrally but were not perfectly aligned, the space between them underwent transtension deformation, causing subsidence of the crust and the formation of the Suoh basin (**Putra & Husein, 2016; Aribowo, 2018**). Furthermore, recent studies indicate that volcanic and geothermal activities in Suoh are strongly influenced by this fault structure. The deep shear zones along the fault facilitate the upward migration of thermal fluids from beneath the surface, making the Suoh area an active geothermal system (**Natawidjaja et al., 2017**). Overall, the GSF acts as the principal structural control governing the formation and evolution of the Suoh basin, influencing its geometric configuration and crustal deformation, as well as its volcanic and geothermal activity. This basin serves as a classic example of the relationship between strike-slip faulting and pull-apart basin formation in an active tectonic setting, analogous to the San Andreas Fault system in southern California (**Bellier & Sébrier, 1994**).

Depression zones coincide with low Bouguer anomalies (blue–purple) that are compatible with porous, altered, or loosely consolidated materials. This association, together with the spatial clustering of geothermal manifestations (red dots) within or along basin margins, suggests that the depressions act as structural traps and preferred pathways for hydrothermal fluids. The proximity of several depressions to volcanic centres (e.g. Mount Sekincau) further indicates a combined volcanic-tectonic origin, where subsidence related to eruptive/explosive activity or shallow intrusion is later amplified by strike-slip deformation. Overall, the depression patterns record the interaction of regional fault kinematics with local volcanism and constitute key indicators of active deformation and potential seismic hazard in West Lampung.

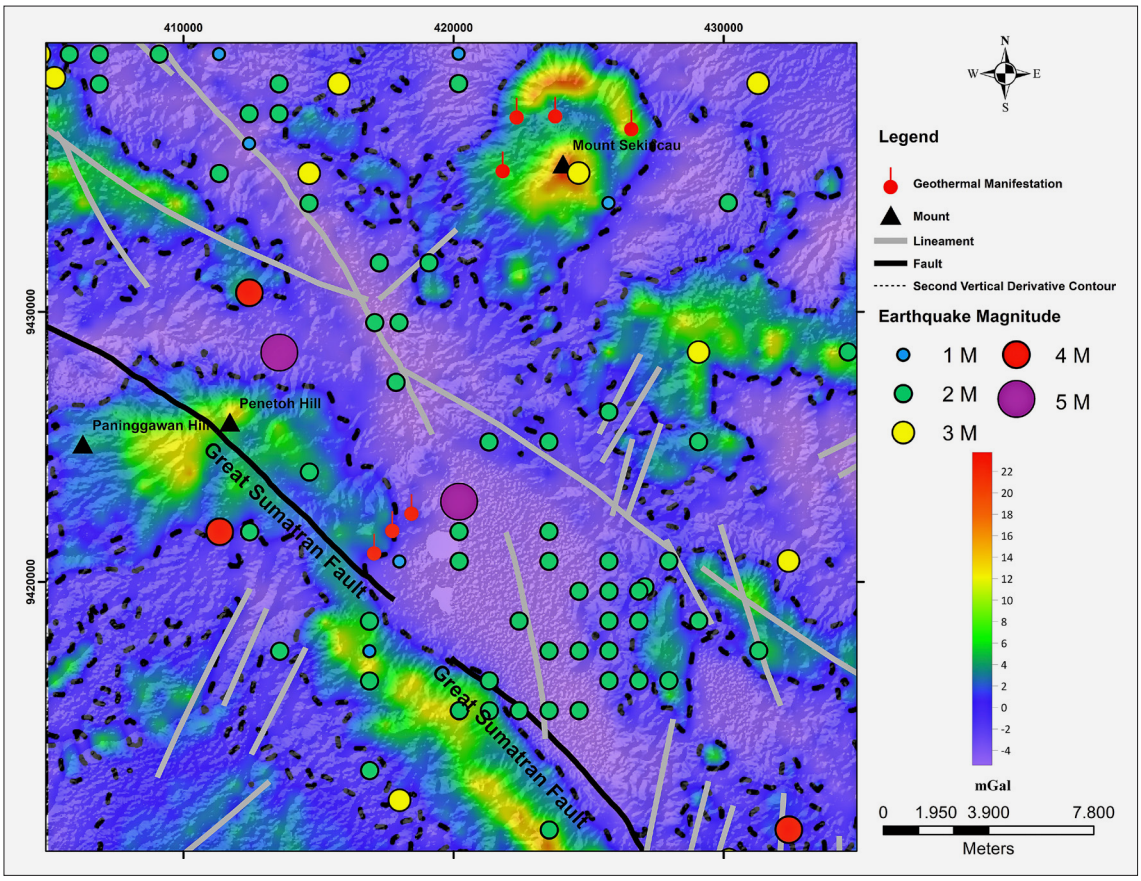


Figure 5: Second Vertical Derivative (SVD) Map of the Study Area

Gravity and seismic observations exhibit a strong correspondence. The CBA reveals a first-order density contrast across the Semangko segment: higher anomalies to the west (interpreted as dense basement or compact volcanic/intrusive rocks) and lower anomalies to the east (young volcanics and Quaternary sediments). Residual and derivative maps (FHD and SVD) delineate NW–SE and NE–SW lineaments consistent with the mapped fault fabric, defining a network of structural weaknesses that focus deformation and accommodate earthquake rupture. Earthquake hypocenters cluster along the Semangko strands and subsidiary faults, indicating that these structures are currently active and capable of generating future events. This interpretation accords with the historical record, including the damaging 1933 earthquake in West Lampung. Taken together, integrated gravity–seismic analysis provides an effective means of resolving subsurface fault architecture in this complex setting and has clear implications for hazard assessment.

4.5. Subsurface Model

The 3-D inversion of the residual field reveals a shallow, high-density anomaly (red–yellow) in the central sector, surrounded by lower-density volumes (blue–green) (see **Figure 7**). The high anomaly is interpreted as a compact intrusive/volcanic body, whereas the low-density envelopes likely represent porous, altered, or mechanically weakened rocks. This juxtaposition produces strong contrasts that correlate with mapped faults and inferred zones of weakness, reinforcing the role of subsurface structure in focusing deformation and seismic hazard in Suoh.

Depth slices and four structural sections extracted from the model (see **Figures 8–9**) clarify these relations. Along line AA′ (see **Figure 9a**), a medium-depth dense body beneath Mount Sekincau is flanked by lower-density domains; several fault planes cut the profile from surface to depth, linking the intrusive high to bounding weakness zones. Line BB′ (see **Figures 8, 9b**) shows a similar pattern near Bukit Pangonan, with a shallow, compact body set between lower-density materials and cross-cut by throughgoing faults. Along CC′ (see **Figure 9c**), the Suoh Depression is expressed as a broad low-density package (≈1.9–2.2 g cm^{-3}) extending to ~5 km depth and bounded laterally by the West and East Semangko faults. This low-density fill is consistent with Quaternary volcaniclastic deposits, deformed rocks, and basin sediments, implying a mechanically weak zone prone to strain accumulation. Line DD (see **Figure 9d**) shows the depression confined between the same major strands, with dominant low densities (2.0–2.3 g cm^{-3}) to ~6 km depth and higher-density flanks (2.45–2.8 g cm^{-3}) that likely correspond to intrusive or basement rocks.

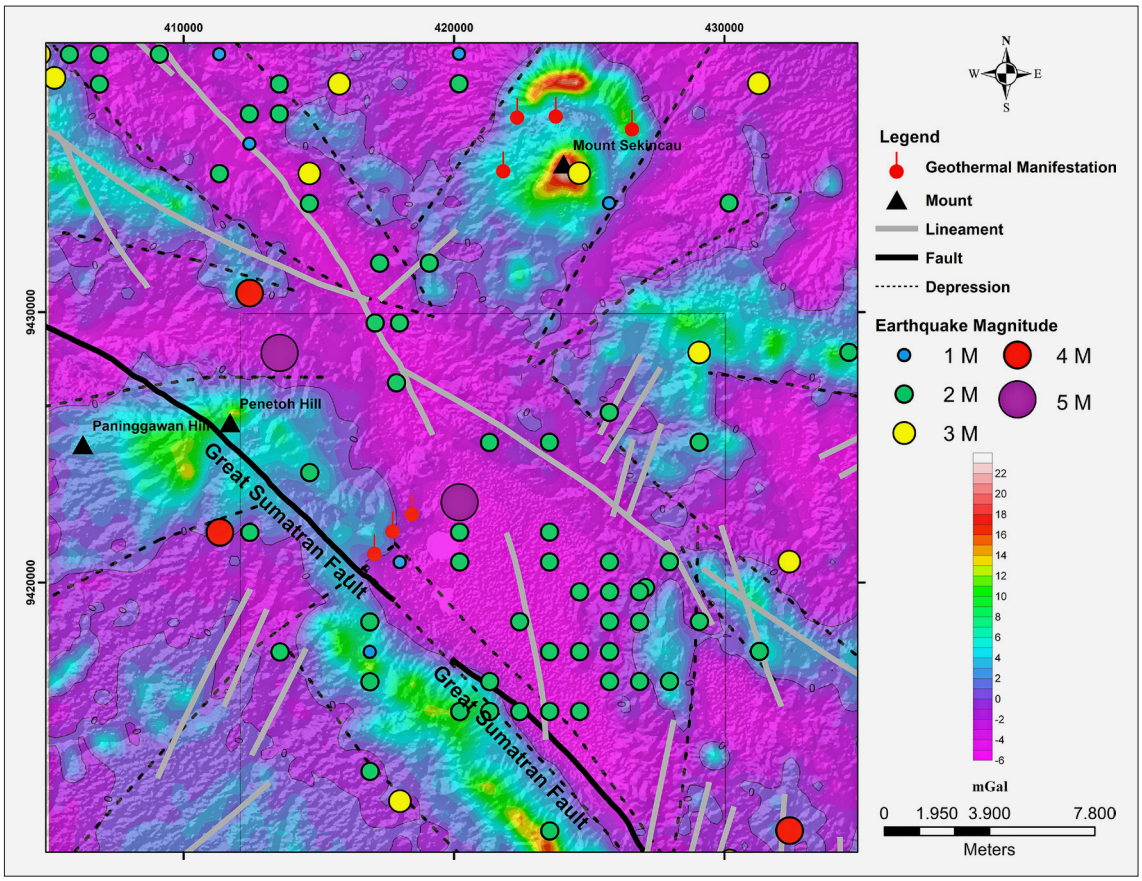


Figure 6: Depression Map of the Study Area

A localised shallow high-density body (>2.6 g cm^{-3}) is identified on the eastern side (horizontal distance ~24–26 km), whereas deeper levels (>6 km) are comparatively homogeneous with moderate to high densities (2.4–2.7 g cm^{-3}), consistent with basement or older compact volcanic rocks. Collectively, the 3-D model corroborates a tectonically controlled architecture: a weak, low-density Suoh Depression bounded by major Semangko strands and punctuated by shallow dense intrusions. This configuration is consistent with ongoing deformation and implies elevated earthquake hazard across the Suoh corridor.

The 3-D inversion highlights a shallow high-density volume (red yellow) in the central sector surrounded by lower-density domains (blue green) (see **Figure 7**). The high is interpreted as a compact intrusive/volcanic body, whereas the lows represent porous, altered or mechanically weakened rocks. This juxtaposition yields strong lateral contrasts that coincide with mapped faults and inferred weakness zones, underscoring the structural controls on deformation and seismic hazards in Suoh. Four orthogonal slices were extracted to interpret subsurface architecture (see **Figures 8–9**). Along line AA′ (see **Figure 9**), a medium-depth dense body beneath Mount Sekincau is flanked by lower-density zones. Several fault planes cut the section from surface to depth, linking the intrusive high with bounding weakness corridors. The configuration shallow intrusion plus adjacent low densities – suggests an actively deforming domain prone to stress accumulation and seismic energy release.

Along line BB′ (see **Figures 8, 9**), a shallow high-density anomaly occurs beneath the western sector near Bukit Pangonan, bounded by lower-density volumes and dissected by throughgoing faults. These structures likely act as deformation pathways and zones of strain localisation, which is consistent with elevated seismic potential. Along line CC′ (see **Figure 9**), the Suoh Depression emerges as a broad low-density package of approximately 1.9–2.2 g cm^{-3} extending to ~5 km depth, bounded laterally by the West Semangko Fault (at ~8–10 km along profile) and the East Semangko Fault (~22–24 km). The low-density fill is compatible with Quaternary volcaniclastic deposits, deformed rocks and basin sediments – materials that are mechanically weak and susceptible to strain accumulation.

Line DD′ (see **Figure 9**) similarly shows the depression confined between the West and East Semangko strands, with dominant low densities of 2.0–2.3 g cm^{-3} to ~6 km depth, flanked by higher-density blocks (2.45–2.8 g cm^{-3}) plausibly corresponding to intrusive or basement rocks. A localised shallow high-density body (>2.6 g cm^{-3}) is resolved on the eastern side at ~24–26 km horizontal distance. At depths >6 km, densities are comparatively homogeneous (2.4–2.7 g cm^{-3}), consistent

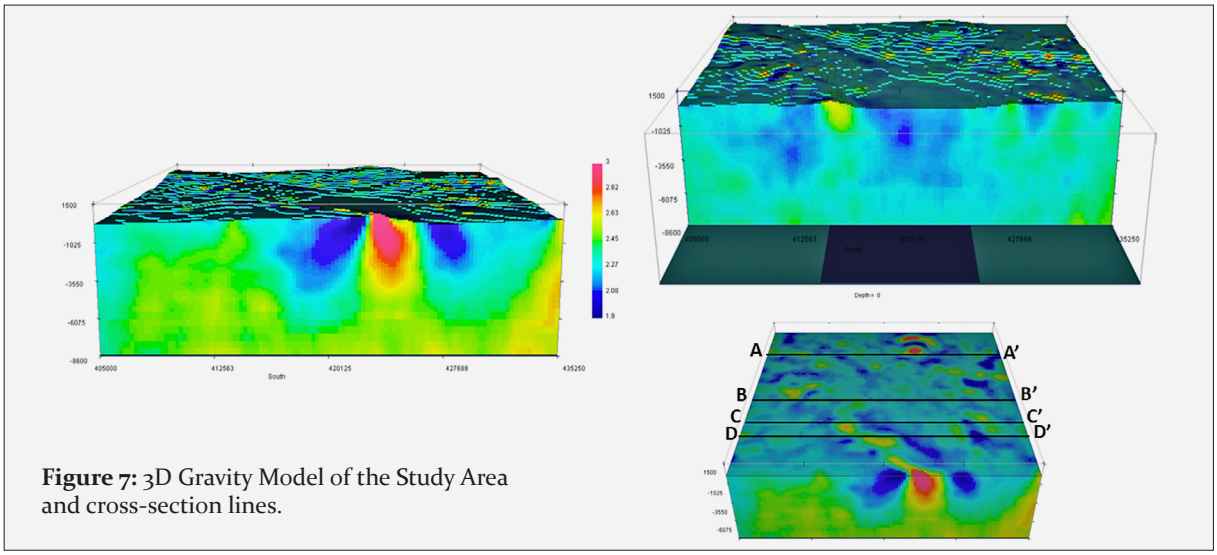


Figure 7: 3D Gravity Model of the Study Area and cross-section lines.

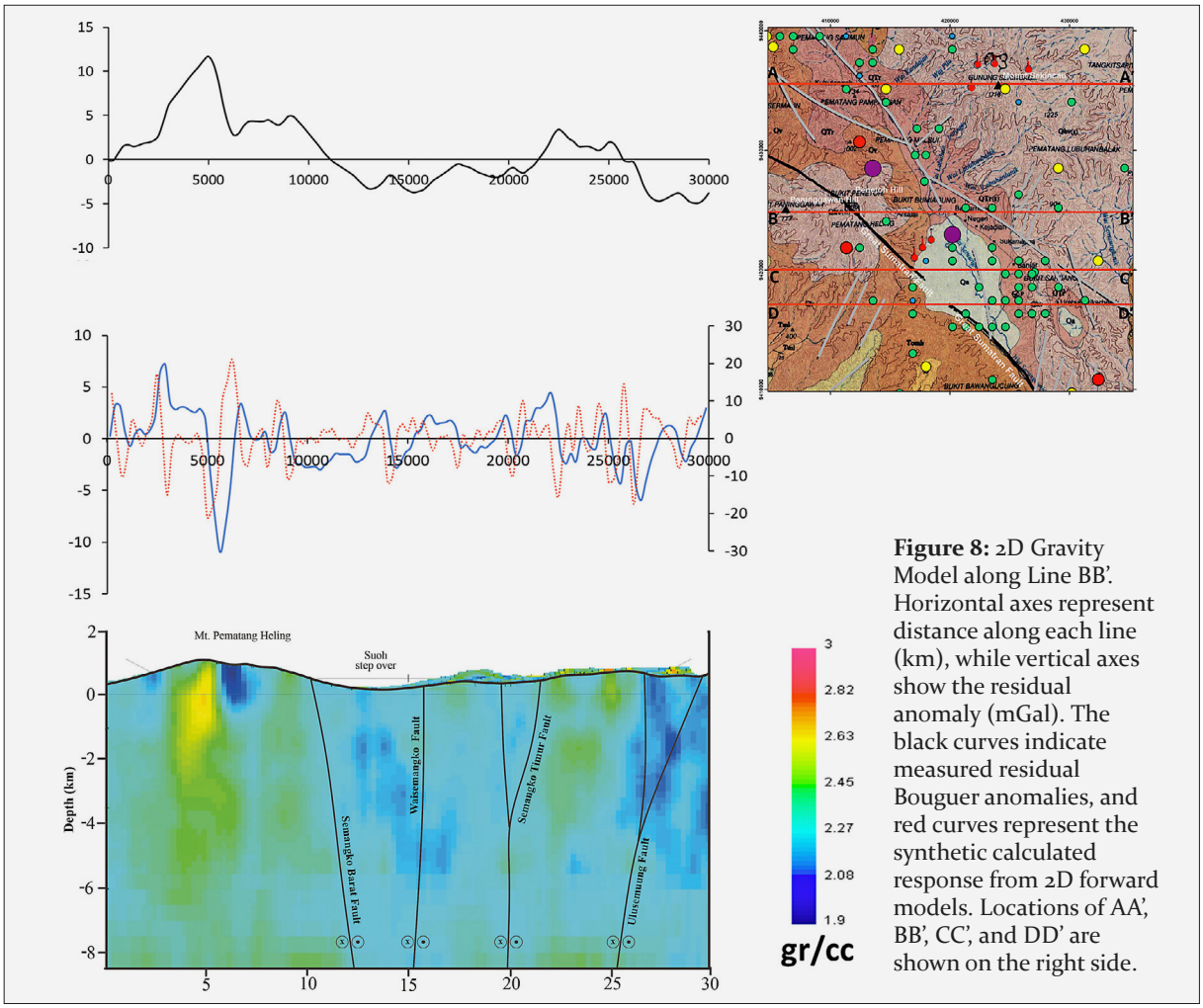


Figure 8: 2D Gravity Model along Line BB'. Horizontal axes represent distance along each line (km), while vertical axes show the residual anomaly (mGal). The black curves indicate measured residual Bouguer anomalies, and red curves represent the synthetic calculated response from 2D forward models. Locations of AA', BB', CC', and DD' are shown on the right side.

with basement or older compact volcanic units. Overall, the 3-D model supports a tectonically controlled architecture: a weak, low-density Suoh Depression bounded by major Semangko strands and punctuated by shallow dense intrusions, consistent with ongoing deformation and elevated earthquake hazard.

The active faults in Sumatra are typically categorised into the northern, central, and southern sectors of the GSF (**Sieh & Natawidjaja, 2000**); the research area is in the southern sector. Suoh developed as a step-over depression between the Kumering and Semangko segments, a releasing geometry that produced a pull-apart basin (**Sieh &**

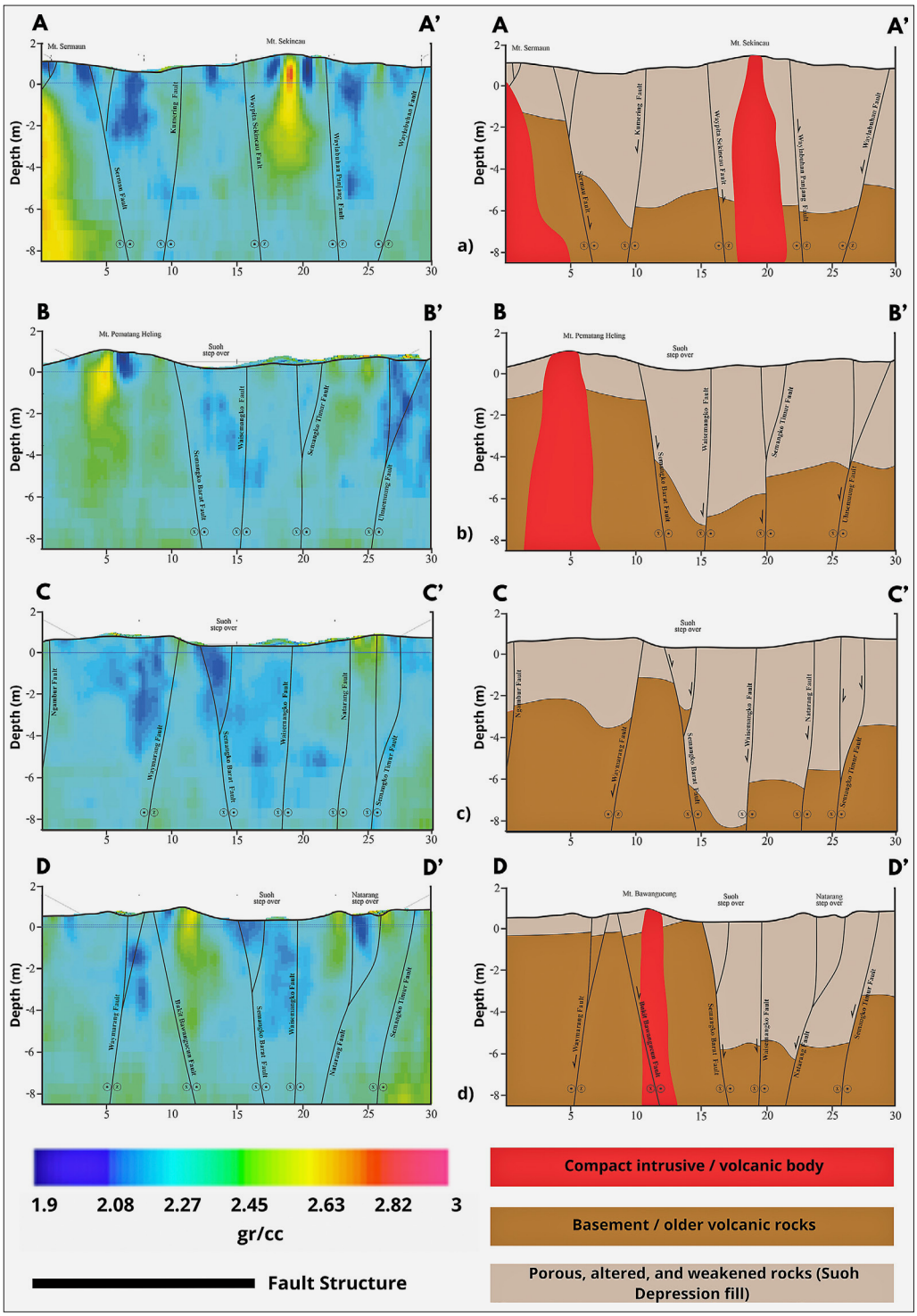


Figure 9: 2D gravity models along four cross-sections: AA', BB', CC', and DD'. The colours represent density contrasts (g cm^{-3}), and the black lines denote interpreted fault boundaries. These models correspond to the profile locations shown in **Figure 8**.

Natawidjaja, 2000; Natawidjaja et al., 2017). Strike-slip segmentation in southern Sumatra has been linked to focused volcanism (**Sutrisno et al., 2019**). In such releasing bends, increased permeability along fault zones, porous syn-tectonic infill and enhanced heat flow due to crustal thinning favour the development of high-temperature geothermal systems (**Sutrisno et al., 2019**). Within the Semangko segment, several pull-apart basins occur; the largest is the Suoh Depression (**Sieh & Natawidjaja, 2000**; **Pramumijoyo, 2008**).

Suoh is situated in the medial to distal volcanic facies, as the depression is filled by Quaternary volcaniclastic sediments that are sourced from nearby volcanic centres, including Mount Sekincau to the NE, Ranau and Sermaun to the north, and Pematang Heling to the NW. Expected lithologies include ash and lapilli tuffs, volcanic breccias, and fluvio-lacustrine conglomerates, sands, and clays. Their low compaction and high porosity are consistent with low gravity values. Geothermal manifestations (hot springs and silica sinter) occur preferentially

along the step-over faults rather than in the central depocentre, reflecting better porosity–permeability in alluvial-fan deposits along fault zones compared with finer-grained basin fills. The likely heat source for the Suoh hot springs is the Pematang Heling volcanic system, as suggested by a shallow magmatic conduit imaged on section B (see **Figure 9**).

5. Conclusions

This study delineates the active fault architecture of Suoh in West Lampung through an integrated analysis of satellite gravity data and regional seismicity. The Complete Bouguer Anomaly (CBA), which represents gravity values corrected for elevation, mass, and terrain effects, together with its residual component that isolates shallow geological sources, provides the primary basis for interpreting subsurface structures.

Derivative-based edge maps, including the First Horizontal Derivative (FHD) that enhances lateral density contrasts and the Second Vertical Derivative (SVD) that emphasises near-surface anomalies, help resolve the geometry of the Semangko segment of the Great Sumatran Fault and several subsidiary NW–SE and NE–SW structures that influence regional morphology and ongoing deformation. Two-dimensional and three-dimensional gravity modelling further reveal strong lateral density contrasts associated with major and secondary faults. Low-density zones correspond to mechanically weak corridors that act as preferred pathways for strain localisation, a process in which tectonic deformation becomes concentrated along specific zones. Consistent with these interpretations, shallow earthquakes cluster along the principal fault strands, demonstrating that tectonic activity in Suoh is ongoing.

Based on the combined lines of evidence, the Semangko segment and its subsidiary splays in the Suoh corridor are classified as active fault systems with clear implications for seismic hazard. These results refine the understanding of the geodynamics of southern Sumatra and provide essential input for earthquake risk reduction, geothermal assessment, and spatial planning in West Lampung.

Acknowledgement

The authors would like to express their gratitude to the Institute for Research and Community Service (LPPM), University of Lampung (Unila), for their administrative support.

Funding

This research was funded by the Ministry of Higher Education, Science, and Technology (KEMDIKTISAINTEK) (Contract Number: 076/C3/DT.05.00/PL/2025) for the Fundamental Research Grant. The authors also thank the West Lampung Government for its support of the research.

6. References

Abdelrahman, K., Pham, L.T., Oliveira, S.P., Duong, V. H., Duy, T. K., Gomez-Ortiz, D., Fnais, M. S & Eldosouky, A. M. (2024). Reliable Tilt-depth estimates based on the stable computation of the tilt angle using robust vertical derivatives. *Scientific reports*, *14*(1), 7392. https://doi.org/10.1038/s41598-024-57314-5

Amin, T. C., Sidarto, S., & Gunawan, W. (1993). *Peta Geologi Lembar Kotaagung, Sumatera skala 1:250.000*. Pusat Penelitian dan Pengembangan Geologi, Bandung.

Al-Khafaji, W. M. S. (2017). Gravity field interpretation for major fault depth detection in a region located Swqa'im/ Iraq. *Baghdad Science Journal*, 14(3), 625–636. https://doi.org/10.21123/bsj.2017.14.3.0625

Aribowo, S. (2018, February). The geometry of pull-apart basins in the southern part of Sumatran strike-slip fault zone. *In IOP Conference Series: Earth and Environmental Science (Vol. 118, No. 1, p. 012002). IOP Publishing.* https://doi.org/10.1088/1755-1315/118/1/012002

Bellier, O., & Sébrier, M. (1994). Relationship between tectonism and volcanism along the Great Sumatran fault zone deduced by SPOT image analyses. *Tectonophysics*, 233(3-4), 215-231. https://doi.org/10.1016/0040-1951(94)90242-9

Bellier, O., Sébrier, M., Pramumijoyo, S., Beaudouin, T., Harjono, H., Bahar, I., & Forni, O. (1997). Paleoseismicity and seismic hazard along the Great Sumatran Fault (Indonesia). *Journal of Geodynamics*, 24(1–4), 169–183. https://doi.org/10.1016/S0264-3707(96)00051-8

Burton, P. W., & Hall, T. R. (2014). Segmentation of the Sumatran fault. *Geophysical Research Letters*, 41(12), 4149–4158. https://doi.org/10.1002/2014GL060242

Dewanto, B. G., Priadi, R., Heliani, L. S., Natul, A. S., Yanis, M., Suhendro, I., & Julius, A. M. (2022). The 2022 Mw 6.1 Pasaman Barat, Indonesia earthquake: Confirmed the existence of the Talamau segment fault based on teleseismic and satellite gravity data. *Quaternary*, 5(4), 45. https://doi.org/10.3390/quat5040045

Elkins, T. A. (1951). The second derivative method of gravity interpretation. *Geophysics*, 16 (1), 29–50. https://doi.org/10.1190/1.1437648

Hirt, C., Claessens, S., Fecher, T., Kuhn, M., Pail, R., & Rexer, M. (2013). New ultrahigh-resolution picture of Earth's gravity field. *Geophysical Research Letters*, 40(16), 4279–4283. https://doi.org/10.1002/grl.50838

Hofi, L. N., Maryanto, S., Susilo, A., Andinisari, R., & Wuryani, S. D. (2024). Fault detection and subsurface model based on gravity data in Pronojiwo, Lumajang, Indonesia. *Evergreen Journal of Novel Carbon Resource Sciences & Green Asia Strategy*, 11(3), 1666–1675. https://doi.org/10.5109/7236820

Hutchings, S. J., & Mooney, W. D. (2021). The seismicity of Indonesia and tectonic implications. *Geochemistry, Geophysics, Geosystems*, 22(9). https://doi.org/10.1029/2021GC009812

Iqbal, M., & Juliarka, B. R. (2019). Analisis kerapatan kelurusan (Lineament Density) sebagai indikator tingkat permeabilitas di Lapangan Panasbumi Suoh-Sekincau, Lampung. *Journal of Science and Applicative Technology*, 3(2), 61–67. https://doi.org/10.35472/jsat.v3i2.212

Iqbal, P., Wibowo, D. A., Raharjo, P. D., Lestiana, H., & Puswanto, E. (2023). The Great Sumatran Fault depression at West Lampung District, Sumatra, Indonesia as geomorphosite for geohazard tourism. *GeoJournal of Tourism and Geosites*, 47(2), 476–485. https://doi.org/10.30892/gtg.47214-1046

Irsyam, M., Widiyantoro, S., Natawidjaja, D. H., Meilano, I., Rudyanto, A., et al. (2017). *Peta Sumber dan Bahaya Gempa Indonesia 2017*. Puslitbang Permukiman, Kementerian PUPR.

Izvoltova, J., Bacova, D., Chromcak, J., & Hodas, S. (2022). Preprocessing of gravity data. *Computation*, 10 (6), 82. https://doi.org/10.3390/computation10060082

LaFehr, T. R. (1991). An exact solution for the gravity curvature (Bullard B) correction. *Geophysics*, 56 (8), 1179–1184. https://doi.org/10.1190/1.1443138

Luo, X., Liu, S., & Tang, X. (2025). A robust method for calculating the vertical derivative of potential fields based on Hilbert transforms. *Scientific Reports*, 15, 18350. https://doi.org/10.1038/s41598-025-99798-9

Marwan, M., Yanis, M., Nugraha, G. S., Zainal, M., Arahman, N., et al. (2021). Mapping of fault and hydrothermal system beneath the Seulawah Volcano inferred from a magnetotellurics structure. *Energies*, 14(20), 6091. https://doi.org/10.3390/en14196091

Moges, G., Alemu, A., & Ejepu, J. (2024). Structural analysis of gravity and magnetic data: Implication for groundwater study in the Ziway, Abijata and Langano lakes corridor and surroundings, central main Ethiopian rift. *Geophysical Journal International*, 240 (3), 1505–1522. https://doi.org/10.1093/gji/ggae461

Moritz, H. (2000). Geodetic Reference System 1980. *Journal of Geodesy*, 74, 128–133. https://doi.org/10.1007/s001900050278

Nowell, D. (1999). Gravity terrain corrections an overview. *Journal of Applied Geophysics*, 42 (2), 117-134. https://doi.org/10.1016/S0926-9851(99)00028-2

Nyalugwe, V. N., Abdelsalam, M. G., Katumwehe, A., Mickus, K. L., & Atekwana, E. A. (2020). Structure and tectonic setting of the Chingale Igneous Ring Complex, Malawi from aeromagnetic and satellite gravity data. *Journal of African Earth Sciences*, 163, 103760. https://doi.org/10.1016/j.jafrearsci.2020.103760

Natawidjaja, D. H., & Triyoso, W. (2007). The Sumatran fault zone – From source to hazard. *Journal of Earthquake and Tsunami*, 1(01), 21-47. https://doi.org/10.1142/S1793431107000031

Natawidjaja, D. H., Bradley, K., Daryono, M. R., Aribowo, S., & Herrin, J. (2017). Late Quaternary eruption of the Ranau Caldera and new geological slip rates of the Sumatran Fault Zone in Southern Sumatra, Indonesia. *Geoscience Letters*, *4*(1), 21. https://doi.org/10.1186/s40562-017-0087-2

Pramumijoyo, S. (2008). Geometri dan Kinematika Sesar Semangko Dam Citra Radar dan Pengamatan Mikrotektonik di Lapangan. *Media Teknik*, *30*.

Parasnis, D. S. (1967). *Principles of Applied Geophysics* (2nd ed.). Methuen & Co., London.

Pham, L. T., Abdelrahman, K., Nguyen, D. V., Gomez-Ortiz, D., Long, N. N., Luu, L. D., … Eldosouky, A. M. (2024). Enhancement of the balanced total horizontal derivative of gravity data using the power law approach. *Geocarto International*, 39(1), 2335251. https://doi.org/10.1080/10106049.2024.2335251

Pranata, B., Ramdhan, M., Hanif, M., Sulaiman, M. I., Maulana, M. P., Wandono, … Setyonegoro, W. (2023). Seismic imaging beneath Sumatra Island and its surroundings, Indonesia, from local-regional P-wave earthquake tomography. *Rudarsko-geološko-naftni zbornik*, 38(3), 119–132. https://doi.org/10.17794/rgn.2023.3.10

Prasetyo, I., Abdul Kadir, W. G., Abdurrahman, D., Dahrin, D., Ibrahim, K., & Kurniawan, A. (2025). New insight into the structural model in Southern Sumatra, Indonesia using gravity and magnetic data: Implications for geothermal resources. *Rudarsko-geološko-naftni zbornik*, 40 (2), 43-60. https://doi.org/10.17794/rgn.2025.2.4

Putra, A. F., & Husein, S. (2016). Pull-apart basins of Sumatran Fault: previous works and current perspectives. *In Proceeding, the 9th Earth National Seminar, 6-7 October 2016*, 42-60.

Rollin, K. E. (1990). *Terrain corrections for gravity stations using a Digital Terrain Model*. British Geological Survey Technical Report WKR 89/8.

Saibi, H., Nishijima, J., Ehara, S., & Aboud, E. (2006). Integrated gradient interpretation techniques for 2D and 3D gravity data interpretation. *Earth, Planets and Space*, 58(7), 815–821. https://doi.org/10.1186/BF03351986

Salem, A., Cheyney, S., Campbell, S., Reuber, K., & Pindell, J. (2014). Integrated 2D forward modeling of seismic and gravity data: A case study from offshore Suriname. *SEG International Proceedings*.

Sarkowi, M. (2010). Identifikasi struktur daerah panasbumi ulubelu berdasarkan analisa data SVD anomali bouguer. *J. Sains MIPA*, 16(2), 111-118.

Sarkowi, M. (2014). *Eksplorasi Gaya Berat*. Graha Ilmu, Yogyakarta.

Sarkowi, M., & Wibowo, R. C. (2021). Geothermal Reservoir Identification based on Gravity Data Analysis in Rajabasa Area Lampung. *Riset Geologi dan Pertambangan Indonesian Journal of Geology and Mining*, *31*(2), 77-97. https://doi.org/10.1088/1742-6596/2110/1/012004

Sarkowi, M., Mulyasari, R., Darmawan, I. G. B., & Wibowo, R. C. (2022). Identification of the Semangko Fault in Sumatra, Indonesia, based on gradient gravity data analysis. *Songklanakarin Journal of Science and Technology*, 44(6), 1503–1509.

Sieh, K., & Natawidjaja, D. (2000). Neotectonics of the Sumatran fault, Indonesia. *Journal of Geophysical Research: Solid Earth*, 105(B12), 28295–28326. https://doi.org/10.1029/2000JB900120

Sumintadireja, P., Dahrin, D., & Grandis, H. (2018). A note on the use of the second vertical derivative (SVD) of gravity data with reference to Indonesian cases. *Journal of Engineering, Technology, and Science*, 50(1), 127–139. https://doi.org/10.5614/j.eng.technol.sci.2018.50.1.9

Supendi, P., Rawlinson, N., Prayitno, B. S., Widiyantoro, S., Simanjuntak, A., Palgunadi, K. H., … Arimuko, A. (2022). The Kalaotoa Fault: A newly identified fault that generated

the Mw 7.3 Flores Sea earthquake. *Seismic Record*, 2(3), 176–185. https://doi.org/10.1785/0320220015

Supendi, P., Widiyantoro, S., Rawlinson, N., Wibowo, A., Priyobudi, P., Palgunadi, K. H., … Sugiharto, A. (2023). Analysis of the 2021 Semangko Bay earthquake sequence in southern Sumatra, Indonesia, using broadband seismic network data. *Seismological Research Letters*, 93(3), 1373–1381. https://doi.org/10.1785/0220210304

Sutrisno, L., Bonte, D., Daud, Y., Smit, J., Beekman, F., Van Wees, J. D., & Purwanto, W. (2019). Assessing the role of pull-apart basins for high-temperature geothermal resources in transcurrent tectonic setting: Sumatra and California compared. In *European geothermal congress* (No. June, pp. 1-8).

Telford, W. M., Geldart, L. P., & Sheriff, R. E. (1990). *Applied Geophysics*. Cambridge University Press.

Wibowo, R. C., Tobing, J. B. L., & Alimuddin. (2022). Geological structure identification using derivative analysis of gravity method. *Journal of Innovation and Technology*, 3(2), 30–36. https://doi.org/10.31629/jit.v3i2.5048

Widiwijayanti, C., Déverchère, J., Louat, R., Sébrier, M., Harjono, H., & Diament, M. (1996). Aftershock sequence of the 1994, Mw 6.8, Liwa earthquake (Indonesia): Seismic rupture process in a volcanic arc. *Geophysical Research Letters*, 23(21), 3051–3054. https://doi.org/10.1029/96GL02048

Witter, J. B., Siler, D. L., Faulds, J. E., & Hinz, N. H. (2016). 3D geophysical inversion modeling of gravity data to test the 3D geologic model of the Bradys geothermal area, Nevada, USA. *Geothermal Energy*, 4(1), 14. https://doi.org/10.1186/s40517-016-0056-6

Yanis, M., Simanjuntak, A. V. H., Abdullah, F., Marwan, M., & Ghani, A. A. (2023). Application of seismicity and gravity observation-based filtering model for mapping a fault structure in Weh Island, Indonesia. *Iraqi Geological Journal*, 56(2A), 260–274.

Zaenudin, A., Karyanto, A., Kurniasih, A., & Wibowo, R. C. (2021). Analisis struktur patahan daerah Suoh menggunakan metode gaya berat dan penentuan kerapatan patahan. *Positron*, 11(2), 95–103. https://doi.org/10.26418/positron.v11i2.48461

SAŽETAK

Integrirani gravimetrijsko-seizmički pristup kartiranju rasjeda u depresiji Suoh na Sumatri

Depresija Suoh (Zapadni Lampung, južna Sumatra) aktivni je vulkanski bazen duž Velikoga sumatranskog rasjeda (GSF), karakteriziran visokom seizmičnošću i aktivnim geotermalnim manifestacijama. U okviru ovoga istraživanja integrirani su podatci satelitske gravimetrije i regionalne seizmičnosti kako bi se ispod površine odredila struktura rasjeda koji kontrolira deformacije u Suohu. Korišteno je 3098 gravimetrijskih točaka iz GGMPlus modela te topografski podatci iz 30 m SRTM DEM-a. Podatci o potresima prikupljeni su iz BMKG kataloga (1900. – 2024.). Obrada gravimetrijskih podataka uključivala je izračun potpune Bouguerove anomalije (CBA), odvajanje regionalnih i rezidualnih komponenti i primjenu filtara za poboljšanje rubova kao što su horizontalni gradijenti i druge vertikalne derivacije. Provedeno je 2D izravno modeliranje i 3D inverzija gustoće kako bi se razriješila geometrija glavnih rasjednih osi. Seizmičnost je analizirana kako bi se potvrdile strukture interpretirane na temelju gravimetrijskih podataka i identificirali aktivni segmenti. CBA varira od ~35 do ~85 mGal, što odražava glavne kontraste gustoće u bazenu Suoh. Zapadni i istočni rasjedi Semangko dva su glavna dijela segmenta Semangko, što pokazuju karte derivacija i rezultati inverzije. Osim toga, postoji i lokalni rasjed Penetoh koji se proteže sjeverozapadno do dubine od oko 6 km. Klasteri potresa podudaraju se s definiranim strukturama, što potvrđuje njihovu trenutačnu aktivnost. Ova saznanja pokazuju da je područje Suoha aktivna ekstenzijska rasjedna depresija kojom upravlja kinematika horizontalnoga rasjedanja. Ažurirana konfiguracija rasjeda pruža ključne podatke za ublažavanje seizmičkoga hazarda, procjenu geotermalnoga potencijala i planiranje korištenja zemljišta u Zapadnome Lampungu.

Ključne riječi:
gravitacijske metode, veliki sumatranski rasjed, seizmičnost, ekstenzijski rasjedni bazen Suoh

Author's contribution

Rahmi Mulyasari (M.Eng., geological engineer with expertise in applied geology, particularly in tectonic geomorphology): performed data processing, interpreted data, and edited the draft. **Muh Sarkowi** (PhD, Professor of Gravity): performed data processing, interpreted gravity data, and edited the draft. **Angga Jati Widiatama** (M.Eng., geological engineer with expertise in applied geology): interpreted geological data and edited the draft. **Hari Wiki Utama** (M.Eng., geological engineer with expertise in applied geology): interpreted geological data and edited the draft. **Andri Kurniawan** (M.Eng., geophysical engineer with expertise in seismology): interpreted data and edited the draft. **Rizky J. Sianturi** (B.Eng., geophysical engineer): interpreted data and edited the draft.
All authors have read and agreed to the published version of the manuscript.